# Spectroscopic and Photophysical Investigations of the Unsaturated Cyclic Trinuclear Clusters $M_3(dppm)_3CO^{2+}$ (M = Pd, Pt). Evidence for Excited-State Guest–Host Chemistry

**Pierre D. Harvey,*[1a] Stephan M. Hubig,[1b] and Tom Ziegler[1c]**

Département de chimie, Université de Sherbrooke, Sherbrooke, Québec, Canada J1K 2R1, Department of Chemistry, University of Houston, Houston, Texas 77204-5641, and Department of Chemistry, University of Calgary, Calgary, Alberta, Canada T2N 1N4

*Received November 15, 1993*®

Evidence for the guest–host chemistry of the organometallic $M_3(dppm)_3CO^{2+}$ clusters (M = Pd, Pt; dppm = $((C_6H_5)_2P)_2CH_2$) in the excited states has been demonstrated for the first time. The first part of the paper addresses the excited-state electronic and structural properties of the cavity, while the second part deals with the dynamics. First, the lowest energy excited states for both M = Pd and Pt are found to be in the $^3A_2{}^*$ state according to approximate density function theoretical computations. When we monitor the UV–visible band at ~460 nm of the $Pd_3(dppm)_3CO^{2+}$ compound (which corresponds to the nearly degenerate 17e → $7a_2$ and 18e → $7a_2$ electronic transitions) as a function of temperature, the moment band analysis enables us to confirm the M–M antibonding nature of the $7a_2$ MO (which indicates that the cavity in the excited state would increase with the M–M bond lengthening) and to estimate $\Delta Q$ (in these $^1E^*$ states). During the course of these studies the $\nu$(M–M) modes have been measured by Raman spectroscopy: M = Pd, $\nu(a_1)$ = 205 cm$^{-1}$, $\nu$(e) = 143 cm$^{-1}$; M = Pt, $\nu(a_1)$ = 149 cm$^{-1}$, $\nu$(e) = 125 cm$^{-1}$. When $\Delta Q$ is fixed to a reasonable value (0.7 Å) by comparison with "$d^{10}$–$d^{10}$–$d^{10}$" $Ag_3$ and $Cu_3$ cluster systems, the structure of the cavity has been modeled using commercially available SYBIL 5.5. It is found that the dppm-phenyl groups (that described the cavity) gain a larger degree of rotational freedom upon the increase of $\Delta Q$ and that the cavity is not perfectly cylindrical but rather exhibits a local $C_{2v}$ symmetry. Second, nanosecond and picosecond flash photolysis experiments demonstrate that molecular associations between the $Pt_3(dppm)_3CO^{2+}$ clusters and the organic solvent molecules also occur in the excited states via the formation of tightly (major product) and loosely bonded complexes which deactivate in the picosecond and nanosecond time scale, respectively. The cavity is found to be hydrophobic in the ground state (according to the emission lifetime measurements at 77 K for $Pt_3(dppm)_3CO^{2+}$ and also appear to be hydrophobic in the excited state despite the fact that the cavity size increases.

## Introduction

Guest–host interactions have important implications in organic and bioinorganic chemistry and represent the very basis of molecular recognition.[2] In the field of organometallic chemistry, the concept of guest–host interactions is not as developed and seems to be nonexistent in cluster chemistry. A family of trinuclear complexes that exhibit characteristics related to such chemistry are the $M_3(dppm)_3CO^{2+}$ (M = Pd, Pt) systems.[3] X-ray crystallographic studies[3] have revealed that the three metal atoms are encircled by a cylindrical array of phenyl rings ("picket-fence-like") forming a hydrophobic cavity (Chart 1). The thermal addition and oxidative additions of substrates into this cavity have been observed exclusively for small molecules.[4] We also note that the $M_3(dppm)_3CO^{2+}$ complexes exhibit homogeneous catalytic activity in the water gas shift reaction (M = Pt)[5] and electrochemical $CO_2$(g) activation and $H_2$(g) evolution (M = Pd).[6] The antibonding nature of the lowest unoccupied molecular orbital (LUMO)[7] suggests that the M–M bond lengths should increase in the excited states and that the cavity size should also increase, hence, allowing larger substrates to interact more efficiently with the unsaturated face of the clusters (in these states). Such a situation would permit stronger interactions

**Chart 1.** General Structure of the $M_3(dppm)_3CO^{2+}$ Complexes[a]

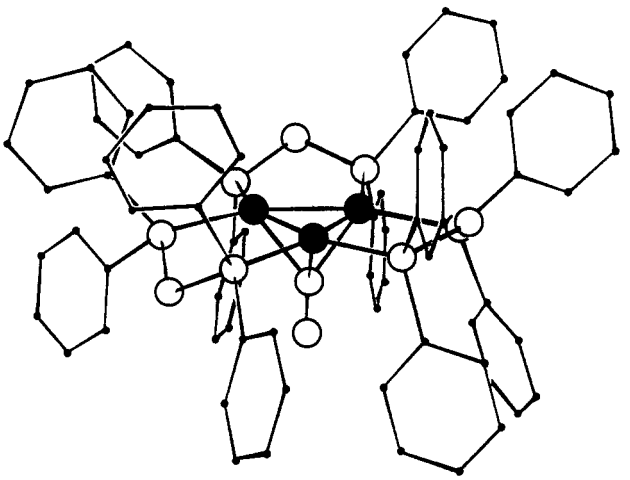

[a] The black atoms are the metal atoms (see ref 3 for details).

* To whom correspondence should be addressed.

® Abstract published in *Advance ACS Abstracts,* July 1, 1994.

(1) (a) Université de Sherbrooke. (b) University of Houston. (c) University of Calgary.

(2) See examples provided in the following references: (a) Connors, K. A. *Binding Constants: The Measurements of Molecular Complex Stability*; Wiley-Interscience: New York, 1987. (b) Gutsche, C. D. *Calixarenes*; Thomas Graham House, Royal Society of Chemistry: London, 1989. (c) Gokel, G. W. *Crown Ethers and Cryptands*; Thomas Graham House, Royal Society of Chemistry: London, 1991. (d) Stoddart, J. F.; Zarzycki, R. *Cyclodextrins*; Thomas Graham House, Royal Society of Chemistry: London, 1992.

(3) (a) Ferguson, G.; Lloyd, B. R.; Puddephatt, R. J. *Organometallics* **1986**, 344. (b) Manojlovic-Muir, L.; Muir, K. W.; Lloyd, B. R.; Puddephatt, R. J. *J. Chem. Soc., Chem. Commun.* **1983**, 1336. (c) Puddephatt, R. J.; Manojlovic-Muir, L.; Muir, K. W. Polyhedron **1990**, *9*, 2767.

(4) (a) Rashidi, M.; Puddephatt, R. J. *J. Am. Chem. Soc.* **1986**, *108*, 7111. (b) Douglas, G.; Manojlovic-Muir, L.; Muir, K. W.; Rashidi, M.; Anderson, G. M.; Puddephatt, R. J. *J. Am. Chem. Soc.* **1987**, *109*, 6527. (c) Schoettel, G.; Vittal, J. J.; Puddephatt, R. J. *J. Am. Chem. Soc.* **1990**, *112*, 6400. (d) Ferguson, G.; Lloyd, B. R.; Manojlovic-Muir, L.; Muir, K. W.; Puddephatt, R. J. *Inorg. Chem.* **1986**, *25*, 4190. (e) Jennings, M. C.; Puddephatt, R. J. *Inorg. Chem.* **1988**, *27*, 4280. (f) Lloyd, B. R.; Bradford, A.; Puddephatt, R. J. *Organometallics* **1987**, *6*, 424. (g) Douglas, G.; Jennings, M. C.; Manojlovic-Muir, L.; Muir, K. W.; Puddephatt, R. J. *J. Chem. Soc., Chem. Commun.* **1989**, 159. (h) Bradford, A. M.; Jenings, M. C.; Puddephat, R. J. *Organometallics* **1989**, *8*, 2367. (i) Manojlovic-Muir, L.; Muir, K. W.; Lloyd, B. R.; Puddephatt, R. J. *J. Chem. Soc., Chem. Commun.* **1985**, 536.

0020-1669/94/1333-3700$04.50/0 © 1994 American Chemical Society

between the metal atoms and the organic substrates prior to photoinduced activation.

We now wish to report our recent experimental and theoretical results that address the excited-state properties of the cavity of the $M_3(dppm)_3CO^{2+}$ clusters (M = Pd, Pt), from both a structural and dynamic point of view. Firmer assignments will also be provided for the electronic bands (using approximate density function theoretical computations). In the case of $Pd_3(dppm)_3CO^{2+}$, first and second moment band analysis of the $^1A_1 \rightarrow {}^1E$ transitions ($17e \rightarrow 7a_2$ and $18e \rightarrow 7a_2$) indicate that the cavity size increases in the excited states ($^1E^*$) and that a Pd–Pd distance ($r(Pd_2)$) is estimated reasonably as ~3.3 Å. During the course of our studies, the low-frequency range of the vibrational spectra was investigated in order to extract the $a_1$ and e modes for the Pd–Pd stretching frequencies, data that are necessary for the band analysis. The excited-state interactions between the clusters and the organic substrates (solvent molecules in this work) were investigated by picosecond flash photolysis spectroscopy at 298 K (M = Pd, Pt) and by the measurement of the emission lifetimes, $\tau_e$ (for M = Pt only). The 298 K excited-state lifetimes strongly depend upon the solvent (except water), while in glass matrices at 77 K the $\tau_e$ values are found to vary to a much lesser extent.

## Experimental Section

**Spectroscopic Measurements.** The absorption spectra were measured on a Hewlett Packard 8452 A diode array spectrometer. The measurements of the UV–vis spectra vs temperature were performed using a homemade assembly: the sample temperature was controlled by a cooled $N_2(g)$ flow going from the bottom to the top of a cylindrical quartz Dewar cell, monitored using a calibrated gold–chromel thermocouple (with an ice bath as reference temperature), and finally allowed ~5 min stabilization prior to each measurement. The luminescence spectra were obtained on a steady-state LS-100 spectrofluorometer from Photon Technology Inc.

The Raman spectra were measured on two different spectrometers. The first one was an Instruments SA Raman spectrometer equipped with a Jobin-Yvon U-1000 1.0-m double monochromator using either the 647.1-nm red line or the 514.5-nm green line of Spectra-Physics krypton and argon ion lasers, respectively, for excitation. The second one was a Bruker IFS 66/CS FT-IR spectrometer coupled with an FRA106FT-Raman module using an Nd:YAG laser (1064-nm excitation) and a Notch filter (cut off ~ 70 $cm^{-1}$). The far-IR spectra were measured on a FT-BOMEM DA 3.002 spectrometer with a resolution of 4 $cm^{-1}$, typically using from 50 to 256 scans.

**Materials.** The $M_3(dppm)_3CO^{2+}$ complexes (M = Pd, $CF_3CO_2^-$ salt; M = Pt, $PF_6^-$ salt) were prepared according to literature procedures.[3] Ethanol (Fisher), methanol (Fisher), acetonitrile (Fisher), benzene (Fisher), toluene (Fisher), butyronitrile (Aldrich), dimethylformamide (DMF; Aldrich), and 2-methyltetrahydrofuran (2-MeTHF; Aldrich) were purified by standard procedures.[8ab] Toluene-$d_8$ and ethanol-$d_6$ were used as received. All spectroscopic measurements were performed immediately after Ar(g) bubbling degassing of the solutions, unless stated otherwise.

**Time-Resolved Measurements.** Picosecond and nanosecond time-resolved measurements were carried out at the Center for Fast Kinetic Research at Austin, TX (CFKR). The set-ups have been previously described.[8c] All samples were degassed before laser flash photolysis by bubbling with nitrogen gas, unless stated otherwise.

**Computational Details.** The reported calculations were all carried out by utilizing the HFS-LCAO program system A-MOL, developed by Baerends et al.[9,10] and vectorized by Ravenek.[11] The numerical integration procedure applied for the calculations was developed by Boerrigter[12] et al. The electronic configurations of the molecular systems were described by an uncontracted triple-$\zeta$ STO basis set[13] for *n*s, *n*p, *n*d, (*n* + 1)s, and (*n* + 1)p on Pd and Pt as well as a double-$\zeta$ STO basis set[14] for carbon (2s, 2p), oxygen (2s, 2p), phosphorus (3s, 3p), and hydrogen (1s). Hydrogens, phosphorus, oxygen, and carbons were given an extra polarization function: $3d_C$ ($\zeta_{3d}$ = 2.5); $3d_O$ ($\zeta_{3d}$ = 2.0); $3d_P$ ($\zeta_{3d}$ = 1.5); $2p_H$ ($\zeta_{2p}$ = 2.0). Levels of lower energy were assigned to the core and treated by the frozen-core approximation. A set of auxiliary[15] s, p, d, f, and g STO functions, centered on all nuclei, was used in order to fit the molecular density and present Coulomb and exchange potentials accurately in each SCF cycle. Energy differences were calculated by combining the local exchange-correlation potential by Vosko[16] et al. with Becke's[17] nonlocal exchange corrections and Perdew's[18] nonlocal correlation correction. The application of approximate density functional theory to organometallic chemistry has been reviewed recently.[19a] The $[M_3(dppm)_3CO]^{2+}$ clusters (M = Pd, Pt) systems were modeled by $M_3(PH_3)_6CO^{2+}$ (M = Pd, Pt) using the geometries given in ref 7. Pictures for the molecular orbital were drawn using EHMO computations (CACAO) as outlined in our earlier work. The detailed description for the graphic programs used in this work can be found in ref 20. The molecular models were built from the crystal structure of $Pd_3(dppm)_3CO^{2+}$ (see text below), and their energies were minimized with SYBIL 5.5 (Triphos Associates, St. Louis, MO). The unmodified TRIPHOS molecular mechanics force fields was used.[21]

## Results and Discussion

**Nature of the Lowest Energy Excited States.** Previously, the nature of the lowest energy excited states was addressed theoretically (using the qualitative extended Hückel molecular orbital calculations: EHMO) and experimentally (via polarization ratio measurements of the excitation spectra).[7] To ensure that our conclusions are correct we have revised the MO data for the $M_3(dppm)_3CO^{2+}$ clusters (M = Pd, Pt). Using the more quantitative type of calculations (HFS-LCAO, density functional theory), the MO energy levels and electronic transitions have been computed for both singlet and triplet excited states (Figure 1, Table 1) taking into account the relativistic effects for M = Pd and Pt. The results (energy level orderings) are very similar to those reported for our previous EHMO computations,[7] and the calculated transition energies compare favorably with the ones obtained experimentally (see Table 1).[7] These calculations now provide further (theoretical) arguments in favor of the lowest energy transition assignment ($13a_1 \rightarrow 7a_2$) and the nature of the excited states.

A brief description of the MO's of interest for this work is provided. The HOMO is the MO $13a_1$ (Figure 1) which is mostly composed of metal d orbitals with some $p_z$ and some C≡O n and $\sigma$ characters. This MO is weakly metal–metal bonding in the $M_3$ plane and is metal–carbon antibonding. The HOMO-1 (18e) and HOMO-2 (17e) are almost entirely composed of in-plane


(5) Puddephatt, R. T. *Can. Chem. News* **1986**, *38*, 6. See also ref 3c.
(6) Harvey, P. D.; Mugnier, Y. To be published.
(7) Harvey, P. D.; Provencher, R. *Inorg. Chem.* **1993**, *32*, 61.
(8) (a) Perrin, D. D.; Armarego, W. L. F.; Perrin, D. R. *Purifications of Laboratory Chemicals*; Pergamon: Oxford, U.K., 1966. (b) Gordon, A. J.; Ford, R. A. *The Chemist's Companion: Handbook of Practical Data, Techniques and References*; Wiley: New York, 1972. (c) Hubig, S. M.; Drouin, M.; Michel, A.; Harvey, P. D. *Inorg. Chem.* **1992**, *30*, 3375.
(9) Baerends, E. J.; Ellis, D. E.; Ros, P. *Chem. Phys.* **1973**, *2*, 41.
(10) Baerends, E. J. Ph.D. Thesis, Vrije Universiteit, Amsterdam, 1975.
(11) Raveneck, W. *Algorithms and Applications on Vector and Parallel Computers*; Rigie, H. J. J., Dekker, Th. J., van de Vorst, H. A., Eds.; Elsevier: Amsterdam, 1987.
(12) Boerrigter, P. M.; Velde, G.; Baerends, E. J. *Int. J. Quantum Chem.* **1988**, *33*, 87.
(13) (a) Snijders, G. J.; Baerends, E. J.; Vernooijs, P. *At. Nucl. Data Tables* **1982**, *26*, 483. (b) Vernooijs, P.; Snijders, G. J.; Baerends, E. J. In *Slater Type Basis Functions for the whole Periodic System*; Internal report; Free University of Amsterdam: Amsterdam, 1981.
(14) (a) Noodleman, L.; Norman, J. G. *J. Chem. Phys.* **1979**, *70*, 4903. (b) Noodleman, L. *J. Chem. Phys.* **1981**, *74*, 5737. (c) Noodleman, L.; Baerends, E. J. *J. Am. Chem. Soc.* **1984**, *106*, 2316.
(15) Krijn, J.; Baerends, E. J. In *Fit functions in the HFS-method*; Internal Report (in Dutch); Free University of Amsterdam: Amsterdam, 1984.
(16) Vosko, S. D.; Wilk, L.; Nusair, M. *Can. J. Phys.* **1990**, *58*, 1200.
(17) Beecke, A. D. *Phys. Rev.* **1988**, *A38*, 2398.
(18) Perdew, J. P. *Phys. Rev.* **1986**, B33, 8822.
(19) (a) Ziegler, T. *J. Pure Appl. Chem.* **1991**, *63*, 873. (b) Ziegler, T.; Versluis, L. *Adv. Chem. Res.* **1991**, *No. 91*, 651. (c) Ziegler, T.; Tschinkec, T. *ACS Symp. Ser.* **1990**, *428*, 277. (d) Ziegler, T.; Snijders, J. G.; Baerends, E. J. *ACS Symp. Ser.* **1989**, *383*, 322. (e) Ziegler, T.; Tschinke, V.; Versluis, L. *NATO ASI Ser.* **1986**, *C176*, 189. (f) Fan, L.; Ziegler, T. *J. Am. Chem. Soc.* **1993**, *115*, 636. (g) Ziegler, T. *Chem. Rev.* **1991**, *91*, 651.
(20) Mealli, C.; Proserpio, D. M. *J. Chem. Educ.* **1990**, *67*, 399.
(21) Clark, M.; Cramer, R. D., III; Van Opdenbosch, N. *J. Comput. Chem.* **1989**, *10*, 982.

**Table 1.** Comparison of the Observed and Computed Transition Energies[a]

| | $Pd_3(dppm)_3CO^{2+}$ | | | | $Pt_3(dppm)_3CO^{2+}$ | | | |
|---|---|---|---|---|---|---|---|---|
| | singlet | | triplet | | singlet | | triplet | |
| excitation | calcd | obsd | calcd | obsd | calcd | obsd | calcd | obsd |
| $13a_1 \rightarrow 7a_2$ | 18 180 | 17 500 | 15 938 | 14 200 | 20 600 | 21 700 | 19 552 | 16 100 |
| $13a_1 \rightarrow 14a_1$ | 26 617 | | 25 577 | | 24 988 | 24 200 | 23 561 | |
| $13a_1 \rightarrow 19e$ | 33 239 | | 32 070 | | 34 562 | 34 700 | 33 498 | |
| $18e \rightarrow 7a_2$ | 21 463 | 20 700 | 19 947 | | 25 135 | 26 200 | 23 811 | |
| $17e \rightarrow 7a_2$ | 22 705 | 21 900 | 21 576 | | 27 989 | 27 600 | 27 037 | |
| $16e \rightarrow 7a_2$ | 27 351 | 27 000 | 26 182 | | 34 167 | 34 700 | 33 005 | |
| $15e \rightarrow 7a_2$ | 29 723 | | 28 585 | | 35 651 | | 35 507 | |
| $14e \rightarrow 7a_2$ | 34 240 | | 33 151 | | 41 919 | | 40 869 | |
| $18e \rightarrow 14a_1$ | 29 900 | | 28 456 | | 29 432 | 30 600 | 27 820 | |
| $17e \rightarrow 14a_1$ | 31 142 | 32 100 | 30 086 | | 32 288 | | 31 045 | |
| $16e \rightarrow 14a_1$ | 35 740 | | 34 691 | | 38 466 | | 37 014 | |
| $15e \rightarrow 14a_1$ | 38 160 | | 37 095 | | 39 950 | | 38 516 | |
| $14e \rightarrow 14a_1$ | 42 740 | | 41 660 | | 46 218 | | 44 878 | |
| $6a_2 \rightarrow 7a_2$ | 27 827 | | 26 585 | | 35 554 | | 33 570 | |
| $18e \rightarrow 19e$ | 36 522 | | 35 701 | | 39 095 | | 28 283 | |
| $17e \rightarrow 19e$ | 37 765 | | 36 814 | | 41 951 | | 41 241 | |

[a] The observed transitions are given in $cm^{-1}$ and are measured at $\nu_{max}$. Experimental conditions: 2-MeTMF as solvent at 77 K.

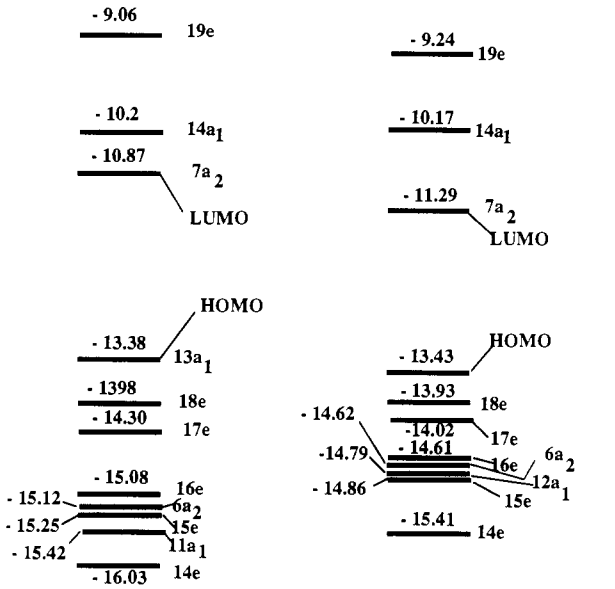


**Figure 1.** MO scheme for the $M_3(PH_3)_6CO^{2+}$ complexes (M = Pd, Pt).

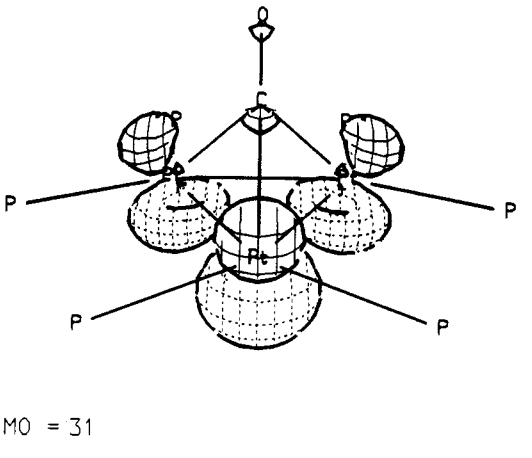


**Figure 2.** Picture of MO no. $14a_1$ for both M = Pd and Pt.

metal d and p orbitals and are formally metal–metal bonding. The LUMO is also strictly composed of metal in-plane d orbitals ($d_{xy}$, $d_{x^2-y^2}$) with some minor $p_x$ and $p_y$ contributions and some phosphorous p components. This MO is formally metal–metal and metal–phosphorous antibonding. A more complete analysis of the MO's and their origins can be found in ref 7 and references therein.

One important difference between the EHMO and LDA results was found for the empty $a_1$ molecular orbital (no. 14), which was located above the empty 19e (molecular orbital no. 19) in our previous EHMO calculations.[7] This orbital now appears only at 1.12 (~9000) and 0.67 eV (~5400 $cm^{-1}$) above the LUMO ($7a_2$). The $14a_1$ MO is mostly composed of metal $p_z$ orbitals (~60%) and some metal $p_x$, $p_y$, and s atomic orbitals. A picture of this MO is shown in Figure 2. The near proximity of the LUMO (no. $17a_2$) and LUMO + 1 (no. $14a_1$) for M = Pt generates an electronic transition $13a_1 \rightarrow 14a_1$ relatively low in energy and close to the $18e \rightarrow 7a_2$ excitation. A more complete list of assignments for the observed bands is provided in Table 1. There are some differences in shape of the UV–vis spectra. Of interest to us are the two intense bands (one band and one shoulder) observed at 77 K for $Pd_3(dppm)_3CO^{2+}$ that are assigned to the $18e \rightarrow 7a_2$ and $17e \rightarrow 7a_2$ transitions. These bands were used for the band analysis (see text below). It was not possible to compute the relative intensities with the AMOL program.

**Vibrational Data.** We have obtained the low-frequency IR and Raman spectra of the complexes in order to identify the $a_1$ and e metal–metal stretching modes ($\nu$(M–M)) assuming a $C_{3v}$ local symmetry (of the $M_3(CO)P_6$ group). These data are necessary for the first and second moment band analysis (see next section). The low-frequency Raman data of the complexes are shown in Figure 3. In this work no force-field analysis was used to separate the M–M stretching bands from other low-frequency bands. The strategy of assignment is based upon the comparison of the IR and Raman spectra, the commonly encountered high intensity of the $\nu$(M–M) modes,[22] and the comparison with literature data for polynuclear Pd and Pt complexes (Table 2),[23] taking into account the M–M bond lengths.

(22) Nakamoto, K. *Infrared and Raman Spectra of Inorganic and Coordination Compounds*, 4th ed.; Wiley: New York, 1986.

(23) (a) Terzis, A.; Strekas, T. C.; Spiro, G. T. *Inorg. Chem.* **1971**, *10*, 2617. (b) Ibers, J. A.; Snyder, R. G. *J. Am. Chem. Soc.* **1962**, *84*, 495. (c) Spiro, T. G.; Templeton, D. H.; Zalkin, A. *Inorg. Chem.* **1968**, *7*, 2165. (d) Preston, H. S.; Mills, J. C.; Kennard, C. H. L. *J. Organomet. Chem.* **1968**, *14*, 447. (e) Rundle, R. E.; Sturdivant, J. H. *J. Am. Chem. Soc.* **1989**, *111*, 1505. (f) Stein, P.; Mahtani, H. K. *J. Am. Chem. Soc.* **1991**, *111*, 3491. (g) Mahtani, H. K. Ph.D. Dissertation, Duquesne University, 1988. (h) Barton, J. K.; Rabinowitz, H. N.; Szalda, D. J.; Lippard, S. J. *J. Am. Chem. Soc.* **1977**, *99*, 2827. (i) Barton, J. K.; Caravana, C.; Lippard, S. J. *J. Am. Chem. Soc.* **1979**, *101*, 7269. (j) Laurent, M. P.; Tewksbury, J. C.; Krogh-Jespersen, M.-B. *Inorg. Chem.* **1980**, *19*, 1656. (k) Mascharak, P. K.; Williams, I. D.; Lippard, S. J. *J. Am. Chem. Soc.* **1984**, *106*, 6428. (l) Lippert, B.; Schöllhorn, H.; Thewalt, U. *Inorg. Chem.* **1987**, *26*, 1736. (m) O'Halloran, T. V.; Roberts, M. M.; Lippard, S. J. *J. Am. Chem. Soc.* **1984**, *106*, 6427. (n) Schubert, V. J.; Neugebauer, D.; Aly, A. A. M. *Z. Anorg. Allg. Chem.* **1980**, *464*, 217. (o) Aly, A. A. M.; Neugebauer, D.; Orama, O.; Schubert, V.; Schmidbaur, H. *Angew. Chem., Int. Ed. Engl.* **1978**, *17*, 125.

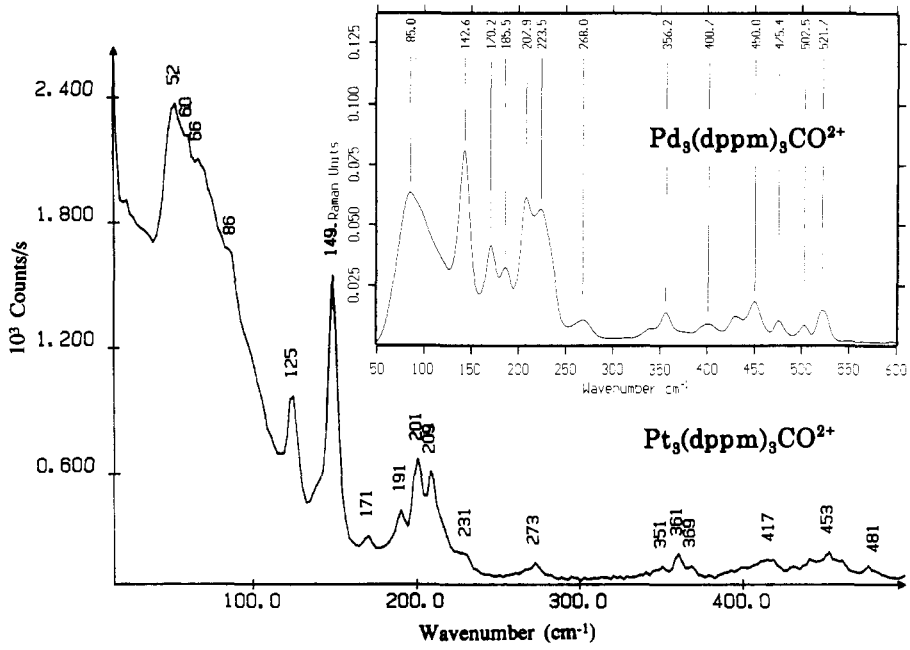


**Figure 3.** Raman spectra of the solid $M_3(dppm)_3CO^{2+}$ complexes at 298 K. M = Pd: Ft-Raman, 200 scans, laser power 70 mW, resolution 4 $cm^{-1}$. M = Pt: micro-Raman, laser excitation 632 nm, laser power 100 mW; 32×, 1 scan, 1 s/pt, 1 $cm^{-1}$/pt.

**Table 2.** Spectroscopic and Structural Data for Various Tri- and Tetranuclear Pd and Pt Clusters

| compds | local sym | ν(M–M) mode sym | ν(M–M)/$cm^{-1}$ | F(M–M)/mdyn $Å^{-1}$ | r(M–M)/Å |
|---|---|---|---|---|---|
| $Pd_3(dppm)_3CO^{2+}$ | $C_{3v}$ | $a_1$ | 205[a] | 1.20[b] | 2.600[c] |
| | | e | 143 | | |
| $Pd_3^-$ | | | 230 ± 30[d] | | 2.70[e] |
| $Pt_3(dppm)_3CO^{2+}$ | $C_{3v}$ | $a_1$ | 149[a] | | 2.634[c] |
| | | e | 125 | | |
| $Pt_3(C_8H_{12})(SnCl_3)_2$ | $D_{3h}$ | $a_{1g}$ | 170[f] | 1.36[f] | 2.58[g] |
| | | $e_g$ | 143 | | |
| $Pt_3^-$ | | | 225 ● 30[d] | | |
| | | | 105 ± 30 | | |
| $((CH_3)_3Pt)_4(OH)_4$ | $T_d$ | $a_1$ | 137[h] | 0.54[h] | 3.43[h] |
| | | $t_2$ | 97 | | |
| | | e | 75 | | |
| $((CH_3)_3Pt)_4Cl_4$ | $T_d$ | $a_1$ | 99[h] | 0.28[h] | 3.73[h] |
| | | $t_2$ | 79 | | |
| | | e | 57 | | |
| $((CH_3)_3Pt)_4I_4$ | $T_d$ | $a_1$ | 88[h] | 0.22[h] | 4.00[h] |
| | | $t_2$ | 65 | | |
| | | e | 48 | | |
| $Pt_4(NH_3)_8(C_5H_4NO)^{5+}$ | $D_{\infty h}$ | $a_{1g}$ | 149[i] | 1.20[i] | 2.774[k] |
| | | $a_{1g}$ | 69 | 0.50[i] | 2.877 |
| $Pt_4(NH_3)_8(C_5H_5N_2O_2)_4^{5+}$ | $D_{\infty h}$ | $a_{1g}$ | 149[i] | | 2.793, 2.810[l] |
| | | $a_{1g}$ | 67 | 2.865 | |
| $Pt_4(en)_4(C_5H_4NO)_4^{5+}$ | $D_{\infty h}$ | $a_{1g}$ | 133[i] | | 2.830, 2.830[m] |
| | | $a_{1g}$ | 67 | | 2.906 |
| $Pt_3(popop)_4^{6-}$ | $D_{\infty h}$ | | 85(R)[n] | (0.80)[o] | (2.925)[o] |
| | | | 147(1R)[n] | | |

[a] This work. [b] Calculated according to eq 1. [c] From ref 3. [d] Erwin, K. M.; Ho, J.; Lineberger, W. C. *J. Chem. Phys.* **1988**, *89*, 4514. [e] Balasubramanian, K. *J. Chem. Phys.* **1989**, *91*, 307. [f] From ref 23a. [g] From ref 23b. [h] From refs 23c–e. [i] From ref 23f. [j] From ref 23g. [k] From refs 23h–j. [l] From refs 23k,l. [m] From ref 23m. [n] From: Dickson, M. K.; Fordyce, W. A.; Appel, D. M.; Alexander, K.; Stein, P.; Roundhill, D. M. *Inorg. Chem.* **1982**, *21*, 3858. [o] The authors in fnt *n* have suggested that the force constant for the Pt···Pt interactions be the same as for $Pt_2(pop)_4^{4-}$. See: Stein, P.; Dickson, M. K.; Roundhill, D. M. *J. Am. Chem. Soc.* **1983**, *105*, 3489 (for $\nu(Pt_2)$). Marsh, R. E.; Herbstein, F. H. *Acta Crystallogr., Sect. B* **1983**, *39*, 280 (for $r(Pt_2)$).

Due to the great laser sensitivity of the samples in solution, it was not possible to perform a systematic resonance Raman spectroscopic investigation (polarization measurements). Nevertheless, our measurements and comparison with the literature have allowed us to assign the two (intense) modes of interest, $\nu(M–M)_{a_1}$ and $\nu(M–M)_e$, to the Raman bands observed at 205 and 143 $cm^{-1}$ for M = Pd and 149 and 125 $cm^{-1}$ for M = Pt, respectively. To further support the assignments, we have obtained the Raman spectrum of $Ag_3(dppm)_3Br_2^+$ [23n,o] for which no Ag--Ag bonding occurs ($r$(Ag--Ag) ~ 3.3 Å). The low-frequency data for the related silver compounds are as follows: 131 sh, 177 br, 220, 251, and 265 $cm^{-1}$. The ones for $Pd_3(dppm)_3CO^{2+}$ are as follows: 143, 170, 185, 207, 220, ~250 sh, 268 $cm^{-1}$. The two highly intense scatterings located at 143 and 207 $cm^{-1}$ in the $Pd_3$ spectrum are not present in the $Ag_3$ one. The Pt data compare favorably with those reported for the structurally related $Pt_3(C_8H_{12})_3(SnCl_3)_2$ [23a] for which the mean $r$(Pt–Pt) value is similar to that reported for $Pt_3(dppm)_3CO^{2+}$.[23b] The frequency ratio $\nu(M–M)_{a_1}/\nu(M–M)_e$ for M = Pd (1.44) is close to the theoretical value $\sqrt{2}/1$ (1.41) for a triangular structure.[24] For M = Pt, this ratio deviates from the theoretical value (1.19; for both $Pt_3(dppm)_3$-

(24) Herzberg, G. *Molecular Spectra and Molecular Structure*; Van Nostrand: New York 1945; Vol. II.

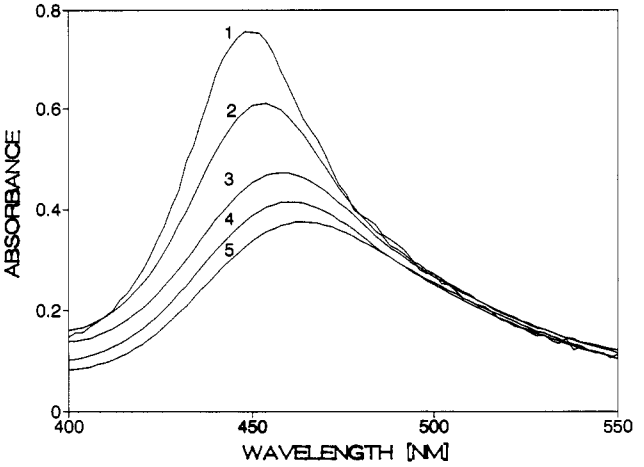


**Figure 4.** UV–visible spectra of $Pd_3(dppm)_3CO^{2+}$ in ethanol vs temperature: (1) 80 K; (2) 150 K; (3) 235 K; (4) 270 K; (5) 300 K.

$CO^{2+}$ and $Pt_3(C_8H_{12})_3(SnCl_3)_2$[23a]) but does not appear to be uncommon; the ratios reported for $Ru_3(CO)_{12}$ and $Os_3(CO)_{12}$ are 1.25 and 1.35, respectively.[25] The average $r$(Pd–Pd) and $r$(Pt–Pt) values are 2.60[3b] and 2.63Å,[3a] respectively. Using an empirical relationship relating the $r$(M–M) distance (in Å) and the metal–metal force constant $F$(M–M) (in mdyn Å$^{-1}$) for M = Pd[26]

$$r(\text{Pd–Pd}) = 0.380 \ln F(\text{Pd–Pd}) + 2.67 \qquad (1)$$

a value of 1.20 mdyn Å$^{-1}$ is computed and is typical for a Pd–Pd single bond (generally ranging from 0.75 to 2.0 mdyn Å$^{-1}$).[26] No empirical relationship of this type has been reported for M = Pt yet, but at a 2.63-Å distance, the $F$(Pt–Pt) value should be comparable to those evaluated for $Pt_2(CO)_2Cl_4^{2-}$ ($r$(Pt–Pt) = 2.699 Å;[27] $F$(Pt–Pt) = 1.84 mdyn Å$^{-1}$ [28]) and $Pt_2(CO)_2Cl_4^{2-}$ ($r$(Pt–Pt) = 2.584 Å;[29] $F$(Pt–Pt) = 2.57 mdyn Å$^{-1}$ [28]). These force constants are greater than those reported for the $M_3(CO)_{12}$ clusters (0.82 for M = Ru, and 0.91 mdyn Å$^{-1}$ for M = Os[25]) which exhibit longer $r$(M–M) values (2.88 Å for M = Os).[30] The rest of the low-frequency vibrational data and proposed assignments are provided in the supplementary material.

**First and Second Moment Band Analysis of the Absorption Spectra.** Using the moment analysis,[31] it is possible on some occasions to reasonably estimate the $\Delta Q$ values (excited-state distortions).[32] During the course of these studies we have observed that both $\lambda_{max}$ and the bandwidth of the low energy bands, in particular for $Pd_3(dppm)_3CO^{2+}$ (18e → $7a_2$, 17e → $7a_2$), experience remarkable decreases in temperature (Figure 4). For singly M–M-bonded binuclear systems, these drastic thermal behaviors are known to be characteristic of M–M dσ → dσ* transitions[32,33] and are attributed[32,33a] to the important Franck–Condon terms. The electronic transitions are generally coupled with relatively low-frequency modes; i.e. $\nu(M_2)$. Miskowski et al.[33a] and more recently our group[32] have used moment analysis[31] to quantify the temperature effect on the dσ → dσ* band for some $d^7$–$d^7$ and $d^9$–$d^9$ complexes, respectively. We are now applying this methodology to the $M_3$ systems. For an allowed transition, the oscillator strength is temperature independent. The normalized first and second moments are $\nu_{max}$ and $m^2$, respectively ($m^2 = (8 \ln 2)^{-1}(\text{fwhm})^2$; fwhm = full width at half-maximum), when the band is Gaussian shaped (which is a good approximation for most cases).

When the ground-state vibrational modes (involved in the Franck–Condon terms) are harmonic oscillators (which is often the case for low-frequency modes), both $\bar{\nu}_{max}$ and $m^2$ follow a temperature dependence of the form in (2), where $k$ = Boltzmann

$$\sum_i A_i \coth\left[\frac{\hbar\omega_i}{2kT}\right] + B \qquad (2)$$

constant, $T$ = temperature, and $\hbar\omega_i$ values are the ground-state vibrational frequencies (for an absorption spectrum). The temperature-independent $B$ term in the first moment equation is related to the electronic transition energy. The $B$ value for the second moment should be either zero or very small according to theory.[31] It has been proposed[33a] that nonzero $B$ values are to be attributed to Franck–Condon-active modes that are too energetic to contribute strongly to the temperature dependence.

The relatively intense (and well isolated) band located ~460 nm in the $Pd_3(dppm)_3CO^{2+}$ spectra (18e → $7a_2$, 17e → $7a_2$) is not resolved into two components in these experiments (ethanol used as solvent). The two bands are separated by ~1200 cm$^{-1}$ only (i.e. ~25 nm; see Table 1 for details). Due to the similar nature of the MO orbitals involved in the electronic transitions, it is reasonable to assume that the temperature dependence for the first ($\bar{\nu}_{max}$) and second moments (fwhm) for both bands are very similar. Therefore the $A$ and $B$ values extracted from this analysis should only be considered as an average for both bands. No attempt to deconvolute these bands was performed.

The plot for $\nu_{max}$ vs $T$ (first moment analysis) is shown in Figure 5. The decrease in $\nu_{max}$ with the temperature will lead to a negative $A$ value, which is indicative of a decease in force constants from the ground to excited states and is consistent with the decrease in bond order in the M–M framework.[7] At first, single active vibrational mode fits were employed. The results for the computed $A$, $B$, and $\hbar\omega_g$ values lead to very large uncertainties. A "two-mode" model was then used (eq 3). Using

$$\bar{\nu}_{max} = A_1 \coth\left[\frac{\hbar\omega_{g1}}{2kT}\right] + A_2 \coth\left[\frac{\hbar\omega_{g2}}{2kT}\right] + B \qquad (3)$$

eq 3, the nonlinear best fit gives $A_1$ = 210 cm$^{-1}$, $\hbar\omega_{g1}$ = 190 cm$^{-1}$, $\hbar\omega_{g2}$ = 140 cm$^{-1}$, and $B$ = 22 700 cm$^{-1}$, where uncertainties have drastically decreased. The $\hbar\omega_1/\hbar\omega_2$ ratio is 1.36, which is not too different from $\sqrt{2}$ (1.41). Changes in $\hbar\omega_1$ and $\hbar\omega_2$ of more than 20% lead to unacceptable fits of the experimental results. When the $A_1$, $A_2$, and $B$ parameters are fixed slightly different from these, the fits again became unacceptable, and the uncertainties obtained for $\hbar\omega_1$ and $\hbar\omega_2$ greatly increase. The $B$ value is related to the electronic transition energy. In this case, the value should be considered as an average between the bands

(25) Quicksall, C. O.; Spiro, T. G. *Inorg. Chem.* **1968**, *7*, 2365.
(26) Perreault, D.; Drouin, M.; Michel, A.; Harvey, P. D. *Inorg. Chem.* **1993**, *31*, 1601.
(27) (a) Brown, M. P.; Puddephatt, R. J.; Rashidi, M.; Manojlovic-Muir, L. J.; Muir, K. W.; Solomun, T.; Seddon, K. R. *Inorg. Chim. Acta* **1977**, *23*, L33. (b) Manojlovic-Muir, L. J.; Muir, K. W.; Solomun, T. *Acta Crystallogr.* **1979**, *B35*, 1237.
(28) Harvey, P. D. Unpublished results.
(29) Modinos, A.; Woodward, P. *J. Chem. Soc., Dalton Trans.* **1974**, 1516.
(30) Corey, E. R.; Dahl, L. F. *Inorg. Chem.* **1962**, *1*, 521.
(31) (a) Markham, J. J. *Rev. Mod. Phys.* **1959**, *31*, 956. (b) Ballhausen, C. J. *Molecular, Electronic Structures of Transition Metal Complexes*; McGraw-Hill; New York, 1979; pp 132–135. (c) Huang, K.; Rhys, A. *Proc. R. Soc. (London)* **1958**, *A204*, 406.
(32) Harvey, P. D.; Murtaza, Z. *Inorg. Chem.* **1993**, *32*, 4721.
(33) (a) Miskowski, V. M.; Smith, T. P.; Loehr, T. M.; Gray, H. B. *J. Am. Chem. Soc.* **1985**, *107*, 7925. (b) Levenson, R. A.; Gray, H. B. *J. Am. Chem. Soc.* **1975**, *97*, 6042. (c) Wrighton, M. S.; Ginley, D. S. *J. Am. Chem. Soc.* **1975**, *97*, 4246. (d) Abrahamson, H. B.; Frazier, C. C.; Ginley, D. S.; Gray, H. B.; Lilienthal, J.; Tyler, D. R.; Wrighton, S. *Inorg. Chem.* **1977**, *16*, 1554. (e) Tyler, D. R.; Levenson, R. A.; Gray, H. B. *J. Am. Chem. Soc.* **1978**, *100*, 7888.
(34) See for example: Stiegman, A. E.; Rice, S. F.; Gray, H. B.; Miskowski, V. M. *Inorg. Chem.* **1987**, *26*, 1112 and references therein.
(35) See for example: Harvey, P. D.; Dallinger, R. F.; Woodruff, W. H.; Gray, H. B. *Inorg. Chem.* **1989**, *28*, 3057.
(36) Perreault, D.; Drouin, M.; Michel, A.; Miskowski, V. M.; Schaefer, W. P.; Harvey, P. D. *Inorg. Chem.* **1992**, *31*, 695 and references therein.
(37) Kirss, R. V.; Eisenberg, R. *Inorg. Chem.* **1989**, *28*, 3372.
(38) Harvey, P. D.; Mugnier, Y. Unpublished results. The EHMO energies for $Pd_3(dppm)_3CO$ for $r$(M–M) ranging from 2.6 to 3.3 Å have been computed; the relative energy order for the MO's remain unchanged.

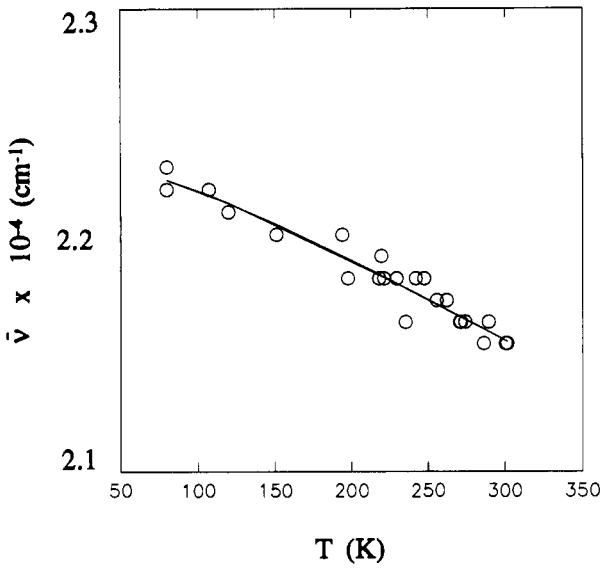


**Figure 5.** Variation of $\bar{\nu}_{max}$ of the $^1E^* \leftarrow {}^1A_1$ band vs temperature. The circles represent the experimental data; the line is the best fitted curve.

and compares favorably with the computed transition energies provided in Table 1. By using a three active Franck–Condon mode model, the uncertainties decreased only slightly (within 10%), and the three $\hbar\omega_{gi}$ values were spread between 200 and 140 cm$^{-1}$. With these observations, we come to the conclusion that the temperature dependence for $\nu_{max}$ (first moment) is best explained by a dominant two Franck–Condon active mode model. The close similarity (within the experimental uncertainties) for $\hbar\omega_{gi}$ (200) and $\hbar\omega_{g2}$ (140 cm$^{-1}$) with the ones obtained by Raman spectroscopy 207 ($a_1$) and 143 cm$^{-1}$ (e) is reassuring, and the assignment for the $\nu$(M–M) $a_1$ and e modes being the two dominant Franck–Condon active modes appear to be reasonably secured.

With two modes, the second moment equation becomes as follows:

$$\frac{(\text{fwhm})^2}{8\ln 2} = A_1 \coth\left[\frac{\hbar\omega_{g1}}{2kT}\right] + A_2 \coth\left[\frac{\hbar\omega_{g2}}{2kT}\right] + B \quad (4)$$

According to theory,[31] $A = S(\hbar\omega_e)^2$, where $S$ is the Huang–Rhys parameter[31c] and where $\hbar\omega_e$ is the excited-state frequency. Knowing that the $S$ value is given by (5),[31] where $\mu$ is the reduced

$$S = \left[\frac{\mu\omega_e^2}{2\hbar\omega_g}\right]\Delta Q^2 \quad (5)$$

mass, $\hbar\omega_g$ is the ground-state vibrational frequency, and $\Delta Q$ is the excited-state distortion, eq 3 becomes

$$(\text{fwhm})^2 = 16\pi^2(\Delta Q)^2\left\{(\nu_{e1})^2\sqrt{\ln 2 \coth\left[\frac{0.72\nu_{g1}}{T}\right]\frac{\mu c}{\hbar\nu_{g1}}} + (\nu_{e2})^2\sqrt{\ln 2 \coth\left[\frac{0.72\nu_{g1}}{T}\right]\frac{\mu c}{\hbar\nu_{g1}}}\right\} + B \quad (6)$$

where $\nu_{ai}$ and $\nu_{ei}$, respectively, are the vibrational frequencies in the ground and excited states given in cm$^{-1}$ units and $c$ is the speed of light. By setting $\nu_{a1} = \sqrt{2}\nu_{e2}$, where the indices 1 and 2 indicate the $a_1$ and e modes, respectively, eq 6 becomes

$$(\text{fmhm})^2 = A\left[\coth\left(\frac{0.72\nu_{g1}}{T}\right) + \frac{\sqrt{2}}{4}\coth\left(\frac{0.72\nu_{g2}}{T}\right)\right] + B \quad (7)$$

with $A$ given by (8), where $\mu = m/3$. Figure 6 shows the graph

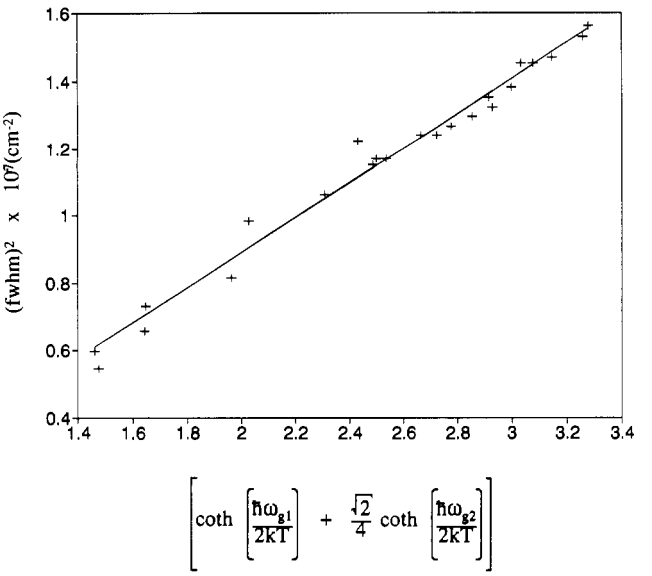


**Figure 6.** Graph of (fwhm)$^2$ vs [coth($\hbar\omega_{g1}/2kT$) + ($\sqrt{2}$/4) coth ($\hbar\omega_{g2}$/$2kT$)] (second moment plot) of the $^1E^* \rightarrow {}^1A_1$ band for $Pd_3(dppm)_3CO^{2+}$ in ethanol. The crosses represent the experimental points; the line is the best fit ($\hbar\omega_{g1}$ = 205 cm$^{-1}$; $\hbar\omega_{g2}$ = 143 cm$^{-1}$).

**Table 3.** Selected $\Delta Q$ values vs $\hbar\omega_{e1}$ for the $^1E^*$ States of $Pd_3(dppm)_3CO^{2+}$

| $\hbar\omega_{e1}$/cm$^{-1}$ [a] | $Q$/Å[b] | $\hbar\omega_{e1}$/cm$^{-1}$ [a] | $Q$/Å[b] |
|---|---|---|---|
| 190 | 0.20 | 130 | 0.45 |
| 180 | 0.235 | 120 | 0.52 |
| 170 | 0.26 | 110 | 0.63 |
| 160 | 0.30 | 100 | 0.76 |
| 150 | 0.34 | 90 | 0.94 |
| 140 | 0.39 | | |

[a] $\hbar\omega_{e1}$ is the excited-state $\nu_e(a_1)$. [b] Calculated using eq 7.

$$A = (\ln 2)16\pi^2(\Delta Q)^2\nu_{ei}^4\left(\frac{\mu c}{\hbar\nu_{g1}}\right) \quad (8)$$

of (fmhm)$^2$ vs the coth function described in eq 7. The least-square linear fit gives $A = 5.20 \times 10^6$ cm$^{-2}$. Equation 8 indicates that $\Delta Q$ and $\nu_{e1}$ are interdependent and can be evaluated when $A$ is known (Table 3). Knowing that the M–M force constant decreases in the excited state, the $\nu_{e1}$ value should be lower than the one in the ground state. Unfortunately the $\nu_{e1}$ value is not known. Generally $\nu_{e1}$ can be extracted from high-resolution UV–vis spectroscopy[34] or from the time-resolved resonance Raman (TRS) spectra.[35] All attempts to obtain such a datum from UV–vis (even at 4 K) and TRS uniformly failed. However, some estimate can be provided. First, diphosphine ligands of the type dppm and dmpm (bis(dimethylphosphino)methane) are capable of bridging two M atoms where no formal bonding occurs between them (such as in the $d^{10}$–$d^{10}$ cases) and can range between 3 and 3.6 Å.[36,37] Second, one should consider the bonding scheme of the LUMO and HOMO. The two-electron reduction (–0.70 vs SSCE, in a 1:1 DMF acetonitrile mixture and 0.1 M LiCl supporting electrolyte)[38] of $Pd_3(dppm)_3CO^{2+}$ reversibly leads to the formation of a red $Pd_3(dppm)_3CO$ complex ($\nu$(CO) = 1967 cm$^{-1}$).[38] These complexes are essentially "$d^{10}$–$d^{10}$–$d^{10}$" compounds where no M–M formal bonding occurs. This is a situation where the $7a_2$ and $13a_1$ MO (Figure 1) are now filled with two electrons each (Figure 7). Considering the first excited electronic configuration for $Pd_3(dppm)_3CO^{2+}$ ($\cdots{}^1(13a_1)^1(7a_2)$), the bond order (zero) should be the same as for the neutral cluster $Pd_3(dppm)_3CO$ ($\cdots{}^2(13a_1)^2(7a_2)$) (Figure 7). The $Pd_2(dppm)_3$ complex is a $d^{10}$–$d^{10}$ compound where no formal Pd–Pd bond occurs in the ground state ($r(Pd_2) \sim 3$ Å),[37] for which the $\nu(Pd_2)$

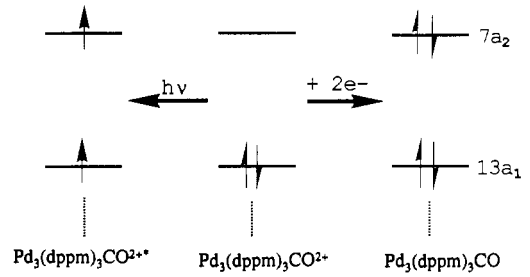


**Figure 7.** Qualitative MO scheme of the HOMO and LUMO for $Pd_3(dppm)_3CO^{2+*}$, $Pd_3(dppm)_3CO^{2+}$, and the neutral species $Pd_3(dppm)_3CO$.

**Chart 2.** Structure of $Ag_3(ddpm)_3Br_2^+$ [a]

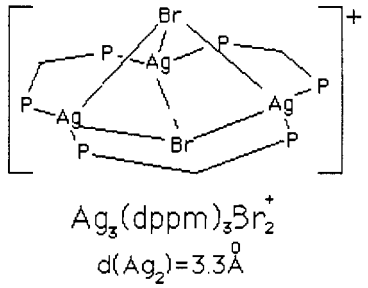


$Ag_3(dppm)_3Br_2^+$

$d(Ag_2) = 3.3$ Å

[a] The phenyl groups are omitted for clarity.

value is found to be 120 $cm^{-1}$ with $F(Pd_2)$ = 0.45 mdyn $Å^{-1}$.[39] If we consider $\nu(Pd_2)$ of 120 $cm^{-1}$ to be the excited state $\nu$(Pd–Pd) ($a_1$) value, then $\Delta Q$ = 0.52 Å (Table 3). $Ag_3(dppm)_3Br_2^+$,[23n,o] $Cu_3(dppm)_3(OH)^{2+}$,[40a] and $Cu_3(dppm)_3Cl_2^+$ [40b] are three closely related compounds for this work where the $Ag_3$ (first compound) and $Cu_3$ triangular frames (third compound) are bicapped by two halide atoms (Chart 2) and the $Cu_3$ center of the second compound is monocapped by a hydroxyl group. These clusters are all "$d^{10}$–$d^{10}$–$d^{10}$" species where no Ag--Ag and Cu--Cu bonding interaction occurs with $r$(Ag--Ag) and $r$(Cu--Cu) average values of 3.3 and 3.2 Å, respectively.

If this structure is accepted as a plausible structure for the excited $^1E^*$ state in $Pd_3(dppm)_3CO^{2+}$, the $\Delta Q$ value would be 0.7 Å. According to Table 3, one should expect $\nu$(Pd–Pd) ($a_1$) in the excited state to be ~105 $cm^{-1}$ if such a structure turns out to be the correct one. It is also important to mention that the $r$(Ag--Ag) values could be somewhat greater because of the more repulsive +3 charge located on the Ag atoms in comparison with +2 charge in the $Pd_3$ cluster. Nevertheless these comparisons lead us to the conclusion that $\Delta Q$ must range between 0.5 and 0.7 Å in the two $^1E^*$ states. The uncertainty appears to be rather large but is acceptable when considering the number of approximations used. The decrease in $\nu$(Pd–Pd) ($a_1$) from the ground (207 $cm^{-1}$) to the excited state (~105–120 $cm^{-1}$) appears large but is comparable to other polymetallic systems. The "closest" (and perhaps only known) system to the $Pd_3$ complex investigated is the "naked" $Cu_3$ molecule. The copper trimer ($D_{3h}$) is known to have both ground- ($^2E'$) and excited-state ($^2E''$) structures that are Jahn–Teller distorted (vibrational–electronic coupling).[41,42] The ground-state ($^2E'$) symmetric stretch is 354 $cm^{-1}$,[43] while the excited-state ($^2E''$) symmetric stretch is 252 ± 5 $cm^{-1}$ with an excited-state bending mode of 149 ± 1 $cm^{-1}$.[44] Unfortunately, no $r$(Cu–Cu) value is reported.

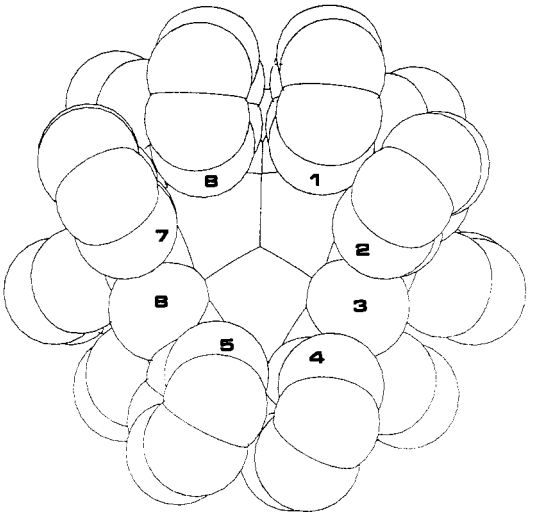


**Figure 8.** View along the $z$-axis of the cavity of a CPK model of the $Pd_3(dppm)_3CO^{2+}$ complex in the ground state, based upon the X-ray structure of $[Pd_3(dppm)_3CO](CF_3CO_2)(PF_6)\cdot 2(CH_3)_2CO$. The H-atoms are not shown for clarity.

There was no attempt to perform the first and second moment band analysis for the $Pt_3(dppm)_3CO^{2+}$ $^1E^* \leftarrow {}^1A_1$ bands. These bands are located near a third lower energy (and fully allowed) band ($^1A_1^* \leftarrow {}^1A_1$; see Table 1 for details) which is different in nature. First, it would be wrong to assume that the slopes for the graph (fwhm)$^2$ vs the coth function for the three bands would be the same. Second, it appears to be practically impossible to deconvolute these three bands with a reasonable degree of reliability, due to their proximity and the fact that these three appear as a shoulder at 298 K.

One other important fact that needs to be addressed is the nature of the lowest energy triplet excited state which is $^3A_2$ (not $^3E^*$). The HOMO ($13a_1$) is partially M–M bonding in comparison with the 18e and 17e MO's, which are strongly bonding.[7,45] The 18e and 17e → $7a_2$ electronic transitions induce larger changes in bond order (perhaps the equivalent of bond order 1 to bond order 0) than the $13a_1$ (HOMO) → $7a_2$ (LUMO) transition. Therefore the excited distortions in the $^3A_2$ excited state should be less important than in the closely located $^3E^*$ states. As a consequence, the cavity size should be smaller in the emissive $^3A_2$ state than in the higher energy $^3E^*$ ones. Due to the forbidden nature of the observed emission ($2 < \tau_e < 18$ μs at 77 K),[7] the applicability of the first and second moment band analysis becomes questionable.[31] For the purpose of this work, we will simply say that $\Delta Q$ in the $^3A_2$ excited state would be $0 < \Delta Q < 0.5$–0.7 Å.

**Modeling of the Excited-State Structure ($^1E^*$).** In order to obtain a qualitative appreciation of the effect of $\Delta Q$ on the cavity size, we have used the commercially available modeling program called SYBYL.[21] Figure 8 shows a CPK model for $Pd_3(dppm)_3CO^{2+}$ (based upon an unreported X-ray structure),[46] in which the C atoms involved in the cavity description have been numbered from 1 to 8. From this figure a tunnel of ~5-Å dimension can

(39) Harvey, P. D.; Gray, H. B. *J. Am. Chem. Soc.* **1988**, *110*, 2145.
(40) (a) Ho, D. M.; Bau, R. *Inorg. Chem.* **1983**, *23*, 4079. (b) Bresciani, N.; Marsich, N.; Nardin, G.; Randaccio, L. *Inorg. Chim. Acta* **1974**, *10*, L5-L6.
(41) Moskovits, M., Ed. *Metal Clusters*; Wiley: New York, 1986; pp 161 and 170.
(42) Howard, J. A.; Preston, K. F.; Sutcliffe, R.; Mile, B. *J. Phys. Chem.* **1983**, *87*, 536.
(43) DiLella, D. P.; Taylor, K. V.; Moskovits, M. *J. Phys. Chem.* **1983**, *87*, 524.
(44) Morse, M. D.; Hopkins, J. B.; Langridge-Smith, P. R. R.; Smalley, R. E. *J. Chem. Phys.* **1983**, *79*, 5316.
(45) (a) Mealli, C. *J. Am. Chem. Soc.* **1985**, *107*, 2245. (b) Evans, D. G. *J. Organomet. Chem.* **1988**, *352*, 397.
(46) The X-ray structure of the mixed salt $[Pd_3(dppm)_3CO](CF_3CO)_2(PF_6)\cdot 2(CH_3)_2CO$ has been obtained from the partial metathesis of the $CF_3CO_2^-$ salt. The structure is very similar to the one reported for $[Pd_3(dppm)_3CO](CF_3CO_2)_2$.[3b] Selected average distances (Å) are as follows: Pd–Pd = 2.594(13), Pd–P = 2.316(15), Pd–C = 2.08(10), C=O = 1.167(19). Provencher, R.; Drouin, M.; Michel, A.; Harvey, P. D. Unpublished results.
(47) Wilkinson, F. *Chemical Kinetics and Reaction Mechanisms*; Van Nostrand Reinhold: New York, 1980.

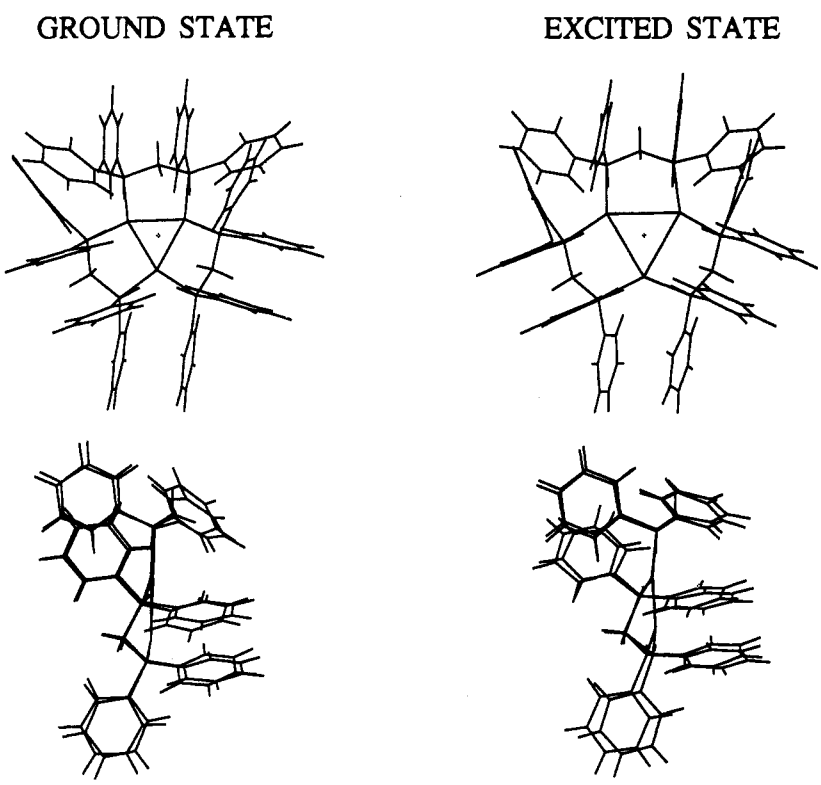


**Figure 9.** Stick models representing the ground-state structure ($^1A_1$; left) and the excited-state (proposed) structure ($^1E^*$; right) for $Pd_3(dppm)_3CO^{2+}$. Top: Upper view of the cavity. Bottom: Side view. The CO group is not shown.

be noticed; this dimension is considered to be the ground-state size for the cavity. For the computations, we have used a $r$(Pd–Pd) value of 3.3 Å (i.e. $\Delta Q = 0.7$ Å) and left the $r$(PdP) distances unchanged as they are not expected to greatly increase in the excited states. The P-atom contributions are found only minor in the LUMO (~6%) and inexistent in the HOMO.[7] The minimization process involved solely the phenyl–phenyl and phenyl–CO steric interactions. The P atoms were also set so as not to be free to move out of the $Pd_3$ plane, since there is no literature evidence for $M_3P_6$ distortion with the addition of atoms or ions inside the cavity. Table 4 compares the H–H distances for the H-atoms located inside the cavity, for both ground- and excited-state structures.

The significant distances are the ones that measure the H–H separations inside the cavity (H1–H4; H5–H8; H2–H7). From these computations, a $\Delta Q$ of 0.7 Å increases the H–H separations by 0.2, 0.3, and 1.2 Å and is a result of rotations of the phenyl groups (nos. 2 and 7) outward from the cavity along the P–C bonds, which are induced by the decrease in inter-dppm phenyl–phenyl steric interactions. In the first approximation, it would have been reasonable to believe that all H–H distances would have changed with about the same magnitude. According to Figure 8, the cavity is *not* cylindrically symmetrical. Considering the $M_3$ center and the six phenyl groups forming the cavity, an approximate $C_{2v}$ (local) symmetry describes the cavity structure with a symmetry plane between H4 and H5. The H–H distance changes are symmetrical with respect to this plane.

The H--H separation of 7.7 Å (H2–H7) in the excited state suggests that molecules of larger dimension may have the potential to interact efficiently with the triangular metallic frame. Due to steric hindrance of the phenyl groups nos. 1, 2, 7, and 8 (Figure 8), the substrate cannot penetrate the cavity perpendicular to the $M_3$ plane. Rather the substrate must penetrate the cavity with an angle closer to the H atoms nos. 4 and 5 (see side view of Figure 9). This affects the nature of the interactions that would take place between a substrate and the metal atoms and the substrate structural selectivity for bindings.

In this work, we did not establish the cavity size in the $^3A_2^*$ state (as already stated), but it appears reasonable to say that the H--H separations H1–H4 and H5–H8 should not be too affected. On the other hand, the H--H distance between the H atoms nos. 2 and 7 will undoubtedly range between 6.5 and 7.7 Å, a distance which depends upon the degree of freedom of the phenyl groups (nos. 2 and 7) to rotate along their P–C bonds. In the absence of a known $\Delta Q$, this H2–H7 distance cannot be estimated reliably in this work, but we will simply accept the fact that the cavity size has increased slightly in the $^3A_2^*$ state, using the data obtained for the $^1E^*$ states as a reference point.

**Table 4.** H···H Distances in the $^1E^*$ and $^1A_1$ states for $Pd_3(dppm)_3CO^{2+}$ [a]

| ground state ($^1A_2$) | | excited state ($^1E^*$) | |
|---|---|---|---|
| H no., H no. | $d$/Å | H no., H no. | $d$/Å |
| 1, 8 | 2.8 | 1, 8 | 3.6 |
| 1, 2 | 2.9 | 1, 2 | 3.2 |
| 2, 4 | 3.8 | 2, 4 | 4.0 |
| 2, 3 | 2.2 | 2, 3 | 2.2 |
| 4, 5 | 3.0 | 4, 5 | 3.4 |
| 5, 7 | 4.5 | 5, 7 | 4.7 |
| 6, 7 | 2.1 | 6, 7 | 2.2 |
| 7, 8 | 2.6 | 7, 8 | 2.9 |
| 2, 7 | 6.5 | 2, 7 | 7.7 |
| 1, 4 | 5.8 | 1, 4 | 6.0 |
| 5, 8 | 5.4 | 5, 8 | 5.7 |

[a] The data for the ground state are those from an X-ray structure.[45] The data for the $^1E^*$ state are those from the modelization computations assuming a $\Delta Q$ of 0.7 Å. The numbering scheme is related to Figure 8.

**Picosecond Flash Photolysis Measurements.** The guest–host chemistry was first demonstrated by Puddephatt et al.[4i] for $Pd_3(dppm)_3CO^{2+}$ with substrate anions such as $CF_3CO_2^-$, $Cl^-$, $Br^-$, and $I^-$. The evidence for this behavior was provided by X-ray crystallography for which two of the four anion–cluster complexes ($X = CF_3CO_2^-$,[3b] $Cl^-$,[4i] and $I^-$ [3c]) were structurally characterized by X-ray (as well as UV–visible spectroscopy). Additions of these anions to a cluster solution induced changes in the UV–visible spectra with the presence of isosbestic points. These spectroscopic analyses demonstrated that the stoichiometry for these associations was 1:1 and that the equilibrium constants vary as $CF_3CO_2^- < Cl^- < Br^- < I^-$.[4i] In the excited state, the

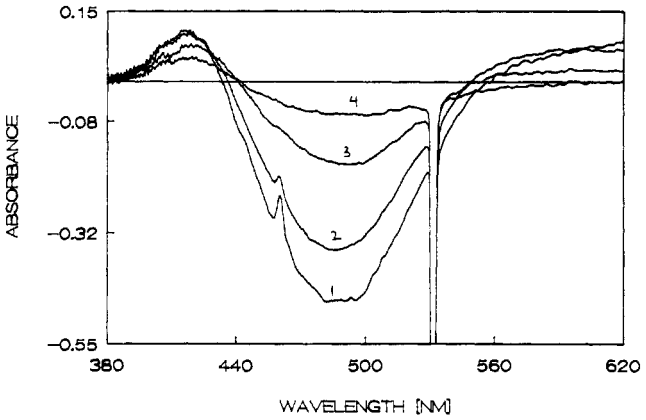


**Figure 10.** Difference absorption spectra of $Pd_3(dppm)_3CO^{2+}$ in ethanol under Ar(g) at 298 K using the 532-nm laser excitation at various delay times: (1) 25 ps; (2) 35 ps; (3) 55 ps; (4) 85 ps.

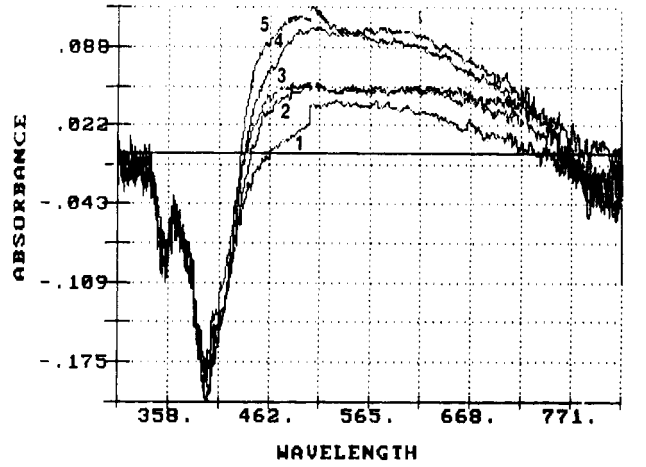


**Figure 11.** Difference absorption spectra of $Pt_3(dppm)_3CO^{2+}$ in toluene under argon at 298 K using the 355-nm laser excitation at various delay times: (1) 200 ps; (2) 120 ps; (3) 75 ps; (4) 50 ps; (5) 25 ps.

increased dimensions of the cavity should allow a larger substrate such as a small organic molecule to penetrate the cavity in order to interact with the $M_3$ center (within the time frame of the transient lifetimes). Due to the lack of luminescence at 298 K, picosecond flash photolysis experiments were performed to monitor these interactions.

Figures 10 and 11 show typical picosecond difference absorption spectra for the $M_3(dppm)_3CO^{2+}$ complexes (M = Pd, Pt). The excitation wavelengths used are the 532- and the 355-nm laser lines for M = Pd and Pt, respectively (355-nm irradiation of the $Pd_3(dppm)_3CO^{2+}$ cluster to photodecomposition). The spectra (Figures 10 and 11) are characterized by the bleaching of the lowest energy absorption bands (~485 nm, M = Pd; 395 nm, M = Pt) and broad and weak transient bands localized at $\lambda > 600$ nm for M = Pd and $\lambda \sim 565$ nm for M = Pt. Within the spectral resolution of our experiments, the shape of the spectra remained the same as a function of delay times. This behavior is consistent with the previously reported observation by Puddephatt et al.,[4i] where $\lambda_{max}$ of both $Pd_3(dppm)_3CO^{2+}$ and $Pd_3(dppm)_3(\mu\text{-Cl})(CO)^+$ were located within ~10 nm.

The excited-state lifetimes for the $Pd_3(dppm)_3CO^{2+}$ samples were measured from the recovery of the ground state at 495 nm (excitation wavelength = 532 nm) since the transient signal ($\lambda > 600$ nm) was too weak. The excited lifetimes are found to be short and somewhat weakly solvent dependent (toluene, 35 ± 10 ps; acetonitrile, 25 ± 10 ps; ethanol, 25 ± 10 ps). The 25–35-ps range is about 1 order of magnitude larger than the singlet lifetime measured for $Pt_2(pop)_4^{4-}$ [48] (8 ps) and appears to be too great to be associated with a singlet state. It also seems very unlikely that

**Table 5.** Picosecond and Nanosecond Flash Photolysis Data for $Pt_3(dppm)_3CO^{2+}$ in Various Solvent Conditions at 298 K under Ar(g)

| | solvent | | | | | |
|---|---|---|---|---|---|---|
| param | $CH_3OH$ | $CD_3OD$ | $CH_3OH$/NaAc(satd) | $C_2H_5OH$ | $C_6H_6$ | $C_5H_5CH_3$ |
| $\tau$(ps)[a] | ≪25 | ≪25 | ≪25 | 30 | 33 | 39 |
| $\tau$(ns)[b] | 310 | 300 | 140 | 190 | 230 | 70 |
| $\phi_{nano}$[c] | ≪5% | ≪5% | <5% | <5% | 35% | 45% |

[a] The experimental uncertainty is ●10 ps. [b] The experimental uncertainty is ±10 ns. [c] $\phi_{nano} = A_{nanosecond}/A_{picosecond}$.

singlet-state species would account for 95% or more of the total transient signal observed for heavy metal complexes. It is therefore believed that these excited-state lifetimes are associated with the triplet state.[49] The excited-state lifetime for a related compound $Pd_2(dppm)_3$ in solution at 298 K, measured by luminescence and by picosecond flash photolysis, is ~6 μs.[50] Despite the fact that the lowest energy excited states are different ($^3(d\sigma^*p\sigma)$ for $Pd_2(dppm)_3$ and $^3((13a_1)^1(7a_2)^1)$ for $Pd_3(dppm)_3CO^{2+}$), the substantially large difference in excited-state lifetimes (25–35 ps vs 6 μs) strongly indicates the presence of specific interactions between a substrate and the chromophore ($Pd_3$ center), promoting further deactivation pathways in the cluster case. These specific interactions are, hence, assigned to a guest–host chemical activity (in the excited state). The very small excited-state lifetime values also lead us to the conclusion that if photoinduced chemical or physical processes are taking place via this transient, they must arise from unimolecular pathways such as a preassociated complex ($Pd_3(dppm)_3CO^{2+}\cdots S$) or an unassociated compound.

The investigations of the $Pt_3(dppm)_3CO^{2+}$ complex turned out to be more informative as the kinetic traces of the transient signal exhibit double exponential decays where both the relative intensities (of the two components) and excited lifetimes ($\tau$) were found to be solvent dependent. Table 5 summarizes the results. To ensure that the $Pt_3(dppm)_3CO^{2+}$ cluster did not exhibit two excited states by which deactivation could take place, we have measured the emission spectra as a function of temperature (4–280 K) for *solid* $[Pt_3(dppm)_3CO](PF_6)_2$. The spectra ($\lambda_{max}$) were temperature independent where only one band was observed and the emission decays were rigorously monoexponential at 77 and 180 K. Therefore, both transients in solutions must originate from the same (triplet) state. In principle, when the specific interactions between a substrate and the chromophore are great, the excited-state lifetimes should be short (see text below). We assign the short-lived species to strongly associated $Pt_3(dppm)_3CO^{2+}\cdots S$ ones. The intensity ratio, $A_{nanosecond}/A_{picosecond}$ (absorbance of the nanosecond species/absorbance of the picosecond species) is small in most cases (<5%), which suggests that there are more transients with strong cluster–substrate interactions than with weak ones.

This observation is consistent with the fact that the cavity size in the excited state increases with respect to the ground state promoting cluster–substrate interactions. It is interesting to note that the increase in $\tau$ (ps) ($CH_3OH < C_2H_5OH < C_6H_6 < C_6H_5CH_3$) supports this model which is essentially based upon substrate

(48) Stiegman, A. E.; Rice, S. F.; Gray, H. B.; Miskowski, V. M. *Inorg. Chem.* **1987**, *26*, 1112.
(49) The nanosecond lifetimes are found to decrease with the increase in laser intensity. Such an observation could be an indication that a triplet–triplet annihilation process is taking place.
(50) (a) Harvey, P. D.; Gray, H. B. *J. Am. Chem. Soc.* **1988**, *110*, 2145. (b) Harvey, P. D.; Dallinger, R. F.; Woodruff, W. H.; Gray, H. B. *Inorg. Chem.* **1989**, *28*, 3057.
(51) One should note that there is relatively little or no isotope effect ($\tau_{ns}$ = 310 nm ($CH_3OH$); $\tau_{ns}$ = 300 ns ($CD_3OD$)) at 298K which indicates that the cluster $CH_3OH$ interactions are weak in the nanosecond species. No information can be obtained from the picosecond species as the lifetimes remain <25 ps (i.e., within the laser pulse widths).

dimensions. Further, the lifetimes of the nanosecond species are also solvent dependent. This behavior is not too surprising since the lifetime ranges (70–310 ns) allow bimolecular processes to occur. To test this hypothesis, the kinetic traces were monitored upon addition of $CH_3CO_2Na$ into $CH_3OH$ solutions of $Pt_3(dppm)_3CO^{2+}$. Knowing that $CF_3CO_2^-$ binds relatively strongly to the $Pd_3$ center in $CH_3OH$ solutions,[3b,4i] it is reasonable to assume that the $CH_3CO_2^-$ anion will also interact with $Pt_3(dppm)_3CO^{2+}$ and hence will influence the excited-state deactivation rate constants. The nanosecond $\tau$ values exhibit very large decreases going from 310 (acetate free) to 140 ns (acetate saturated solution), which was also accompanied with increases in transient signals (~0.01 to ~0.1 A), and clearly indicate that the $CH_3CO_2^-$ does indeed interact with the cluster. There were no changes in the picosecond signals as the decay was already within the laser pulse widths.

A model that is consistent with the proposed guest–host interactions scheme is shown as follows:

$$\begin{array}{ccc} S + M_3(dppm)_3CO^{2+} & \overset{?}{\rightleftharpoons} & [M_3(dppm)_3CO^{2+}\cdots S]^* \\ h\nu \uparrow\downarrow & & h\nu \uparrow\downarrow \\ S + M_3(dppm)_3CO^{2+} & \rightleftharpoons & M_3(dppm)_3CO^{2+}\cdots S \end{array} \quad (9)$$

Here $M_3(dppm)_3CO^{2+}$ + S and $M_3(dppm)_3CO^{2+}\cdots S$ are the weakly (loosely bonded) and strongly interacting species (tightly bonded), respectively. The excited-state equilibrium (marked with ?) has not formally been proven in this work. The possibility exits, but considering the short excited-state lifetimes, this equilibrium would be rapid. For $Pd_3(dppm)_3CO^{2+}$, the absence of observed nanosecond signals indicates that the equilibrium is totally, or almost totally, shifted toward the strongly interacting species.

The diffusion rate constants typically range between $10^9$ and $10^{10}$ $s^{-1}$ $M^{-1}$ for common organic solvents.[47] The pseudo-first-order rate constants for the diffusion (obtained by dividing the rate constants by the solvent concentration) range from ~$10^8$ to $10^9$ $s^{-1}$. The nanosecond species deactivation rate constants are observed in the $1.4 \times 10^7$ $s^{-1}$ to $3.2 \times 10^6$ $s^{-1}$ range (Table 5) and are 1–3 orders of magnitude lower than the diffusion limit, which indicates that the excited-state deactivations of the nanosecond species are relatively slow processes. On the other hand, the picosecond species exhibit rates of $2.6 \times 10^{10}$ $s^{-1}$ to $4 \times 10^{10}$ $s^{-1}$ and are well outside the solvent diffusion limit. Such an observation is consistent with the tightly-bonded substrate–cluster model.

**Quenching $O_2$.** Attempts to quench the nanosecond transient species by bubbling $O_2$(g) into the solutions failed ($[O_2]_{satd}$ ~ $10^{-2}$ M in common organic solvents).[52] The picosecond species are not quenched by $O_2$ due to the rather fast deactivation kinetics (see for example Figure 12). The results for the nanosecond species show that the excited state lifetimes are rigorously oxygen insensitive as verified for three solvent systems (protic $C_2H_5OH$ and $CH_3OH/H_2O$, 1:1, and aprotic $C_6H_5CH_3$). It seems obvious that the access of $O_2$ to the transient chromophore ($M_3$ center) is sterically hindered via the cavity or that $O_2$ is a weak binding substrate. This important result indicates that the cavity of the nanosecond species is indeed filled by a solvent molecule and confirms, in part, our model (eq 9).

**Interactions with Water.** The kinetic trace of a 1:1 water/$CH_3OH$ mixture containing $Pt_3(dppm)_3CO^{2+}$ ($Pt_3(dppm)_3CO^{2+}$ is water insoluble) indicates that $\tau_{ns}$ is 590 ns (at low laser power). If it is assumed that the cluster–protic substrate interactions increase with the decrease in $\tau_{ns}$ ($\tau_{ns}$ = 310 and 190 for $CH_3OH$ and $C_2H_2OH$, respectively), the 1:1 water/$CH_3OH$ mixture appears to be the "least interacting" solvent system investigated, suggesting that the hydrophobic properties of the cavity in the excited state remain. The results do not indicate, however, that the water molecules do not penetrate the cavity but somehow decrease the capacity for the $CH_3OH$ molecules to interact with the cavity (H-bonding?). The nanosecond kinetic trace is monoexponential.

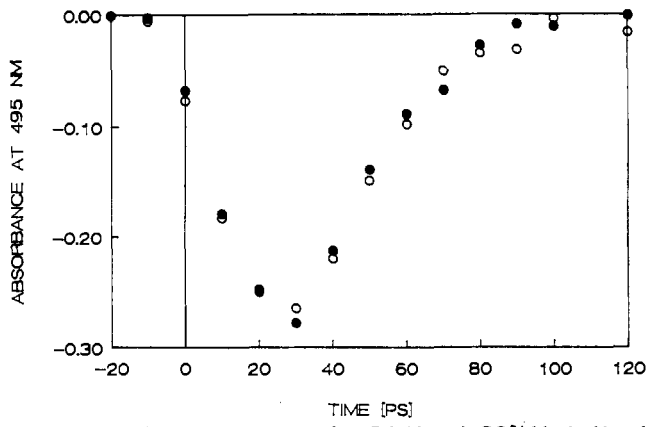


**Figure 12.** Typical recovery curves of the $Pd_3(dppm)_3CO^{2+}$ bleched band (495 nm) using $C_2H_5OH$ as solvent at 298 K (● = under Ar(g); ○ = under $O_2$(g)). Experimental condition: $\lambda_{exc}$ = 355 nm, 25-ps pulse, 11 mJ/pulse.

**Table 6.** 77 K Emission Lifetime and Spectroscopic Data for $Pt_3(dppm)_3CO^{2+}$

| solvent | $\tau_e/\mu s$ | $\lambda_{max}/nm^a$ |
|---|---|---|
| $C_6H_5CH_3$ | 10.2 ± 0.5 | 675 ± 5 |
| $C_6D_5CD_3$ | 8.5 ± 0.5 | |
| $CH_3OH$ | 10.9 ± 0.5 | 675 ± 5 |
| DMF | 12.8 ± 0.8 | 680 ± 5 |
| *i*-PrOH | 13.5 ± 0.3 | 660 ± 6 |
| 2-MeTHF | 13.9 ± 0.2 | 630 ± 5 |
| PrCN | 14.0 ± 0.4 | 650 ± 5 |
| $C_2H_5OH$ | 18.0 ± 0.1 | 640 ± 5 |

[a] Corrected for PMT detection.

**Interactions with Hydrophobic Substrates.** It is also interesting to point out that $\tau_{ns}(C_6H_6)$ decreases from 230 ns to 70 ns for $\tau_{ns}(C_6H_5CH_3)$ which suggests that the methyl group must interact substantially with the $M_3$ center in the excited state. This model would be consistent with the known guest–host chemistry[53] between toluene and calix[4]arenes established from X-ray crystallographic studies where the methyl group is found to point down in the cavity.

**Emission Spectra and Lifetimes at 77 K.** At lower temperatures the molecular associations should be favored. The emission spectra and lifetimes ($\tau_e$) of $Pt_3(dppm)_3CO^{2+}$ have been investigated at 77 K (the data are summarized in Table 6). The $\lambda_{max}$ values are found to be solvent dependent (not temperature dependent) with shifts up to 40 nm. These shifts are too great to be associated with a normal solvent effect and must be linked with the guest–host chemistry described. The $\tau_e$ values also exhibit an unusual variation, where the $\tau_e$ values range from 10.2 to 18.0 $\mu$s (for nondeuterated solvents). The key feature in these studies is the fact that *all* emission decays rigorously obey a monoexponential law, which indicates that only one species is responsible for the emission and that it is the cluster–solvent associated species.

The $\tau_e$ value for the toluene solvent (10.2 $\mu$s) is found to be somewhat smaller than that found for the alcohol solvents ($CH_3OH$, 10.9; $C_2H_5OH$, 18.0 $\mu$s), with the difference that $\tau_e(CH_3OH) < \tau_e(C_2H_5OH)$, and may reflect the difference in H-bond schemes between $CH_3OH$ and $C_2H_5OH$. Additions of water (up

(52) (a) Stephen, H.; Stephen, T. *Solubilities of Inorganic and Organic Compounds*; The MacMillan Co.: New York, 1963; Vol. 1. (b) Murov, S. L.; Carmichael, I.; Hug, G. L. *Handbook of Photochemistry*, 2nd ed.; Marcel Dekker: New York, 1993; p 289.

(53) Bott, S. G.; Coleman, A. W.; Atwood, J. L. *J. Am. Chem. Soc.* **1986**, *108*, 1709.

to 10%) in all the solvents investigated did not change $\tau_e$ (within the experimental uncertainty) and the $\lambda_{max}$ values, which indicates that the cavity is strictly hydrophobic in the ground state *prior* to freezing the solvent at 77 K. The only observed effect is the expected cracking of the solvent glasses at 77 K. These experiments did not exceed the 10% amount of water in order to avoid the precipitation of the complexes upon the decrease in solubility with decreasing temperature and to avoid formation of "snow" at 77 K which complicates the measurements. The $\tau_e$ value using $C_6D_5CD_3$ as a solvent decreased from 10.2 to 8.5 $\mu$s ($C_6H_5CH_3 \rightarrow C_6D_5CD_3$). This isotope effect is somewhat greater than the one previously described for the flash photolysis studies[51] and may be associated with the fact that guest–host interactions are very likely to be favored at lower temperatures as previously stated.

There has been no investigation for the $Pd_3(dppm)_3CO^{2+}$ species since the emission intensity is too small for any accurate and systematic study; $\phi_e(Pd_3(dppm)_3CO^{2+}) < 0.001$.[7]

## Concluding Remarks

This work is divided into two sections. In the first part, we have described the electronic and structural features that characterize the excited-state cavity of the $M_3(dppm)_3CO^{2+}$ clusters (M = Pd, Pt), where we find that the cavity size depends upon both $\Delta Q$ and the relative rotational freedom of the dppm-phenyl groups. The parameters ($\Delta Q$ and rotational freedom of the dppm phenyls) are inter-related. The computed H--H distances describing the interior of the cavity do not increase symmetrically (due to the apparent $C_{2v}$ local symmetry of the cavity) in the excited state, and they design a specific geometric pattern for cluster–substrate interactions for larger substrates, such as benzene and toluene. Such a phenomenon appears to be a very convenient feature for the design of selective photoinduced bond activation in large organic substrates. In the second part, the guest–host interactions in the excited states (for $Pt_3(dppm)_3CO^{2+}$) have been demonstrated for the first time and have been characterized by picosecond and nanosecond flash photolysis (at 298 K) and emission spectroscopy (at 77 K). The cavity, which is found to be rigorously hydrophobic in the ground state, also appears to keep this property in the excited state. Further studies are in progress in the area.

**Acknowledgment.** This research was supported by the NSERC, the FCAR, and the Ministère de l'éducation du Québec (Action structurante en électrochimie). P.D.H. thanks Mrs. J. Hellman (Brucker) and Professor André Michel (U. de Sherbrooke) for the measurements of some FT-Raman spectra and for technical assistance in the modeling computations, respectively. Dr. Z. Murtaza is acknowledged for measuring the UV–vis spectra as a function of temperature.

**Supplementary Material Available:** Table S1, listing the low-frequency vibrational data and assignments for the $M_3(dppm)_3CO^{2+}$ complexes (M = Pd, Pt) (1 page). Ordering information is given on any current masthead page.